HHS Public Access

Author manuscript

J Magn Reson Imaging. Author manuscript; available in PMC 2020 April 21.

Published in final edited form as:

J Magn Reson Imaging. 2019 November ; 50(5): 1504–1513. doi:10.1002/jmri.26765.

Cerebral Circulation Time Derived From fMRI Signals in Large Blood Vessels

Jinxia (Fiona) Yao, BS[1], **James H. Wang, BS**[1], **Ho-Ching (Shawn) Yang, MS**[1], **Zhenhu Liang, PhD**[1,2], **Aaron A. Cohen-Gadol, MD**[3], **Vitaliy L. Rayz, PhD**[1], **Yunjie Tong, PhD**[1,*]

[1]Weldon School of Biomedical Engineering, Purdue University, West Lafayette, Indiana, USA

[2]Institute of Electrical Engineering, Yanshan University, Yanshan, China

[3]Indiana University School of Medicine, Department of Neurosurgery and Goodman Campbell Brain and Spine, Indianapolis, Indiana, USA

Abstract

Background: The systemic low-frequency oscillation (sLFO) functional (f)MRI signals extracted from the internal carotid artery (ICA) and the superior sagittal sinus (SSS) are found to have valuable physiological information.

Purpose: 1) To further develop and validate a method utilizing these signals to measure the delay times from the ICAs and the SSS. 2) To establish the delay time as an effective perfusion biomarker that associates with cerebral circulation time (CCT). 3) To explore within subject variations, and the effects of gender and age on the delay times.

Study Type: Prospective.

Subjects: In all, 100 healthy adults (Human Connectome Project [HCP], age range 22–36 years, 54 females and 46 males), 56 healthy children (Adolescent Brain Cognitive Development project) were included.

Field Strength/Sequence: Echo planar imaging (EPI) sequence at 3T.

Assessment: The sLFO fMRI signals from the ICAs and the SSSs were extracted from the resting state fMRI data. The maximum cross-correlation coef ficients and their corresponding delay times were calculated. The gender and age differences of delay times were assessed statistically.

Statistical Tests: *T*-tests were conducted to measure the gender differences. The Kruskal–Wallis test was used to detect age differences.

Results: Consistent and robust results were found from 80% of the 400 HCP scans included. Negative correlations (–0.67) between the ICA and the SSS signals were found with the ICA signal leading the SSS signal by ~5 sec. Within subject variation was 2.23 sec at the 5% signi ficance level. The delay times were not signi ficantly different between genders ($P = 0.9846$, $P =$

*Address reprint requests to: Y.T., Weldon School of Biomedical Engineering, Purdue University, West Lafayette, Indiana, 47907. tong61@purdue.edu.

Additional supporting information may be found in the online version of this article

0.2288 for the left and right ICA, respectively). Signi ficantly shorter delay times (4.3 sec) were found in the children than in the adults ($P < 0.01$).

Data Conclusion: We have shown that meaningful perfusion information (ie, CCT) can be derived from the sLFO fMRI signals of the large blood vessels.

Level of Evidence: 1

Technical Efficacy Stage: 1

FUNCTIONAL MAGNETIC RESONANCE IMAGING (fMRI) is widely used in neuroscience for exploring brain functions and networks. The blood oxygen level-dependent (BOLD) is the main contrast used in fMRI, which relies on the change in the concentration of deoxyhemoglobin in the blood.[1,2] Therefore, the BOLD fMRI signal is a blood-related signal that indirectly detects neuronal activations through neurovascular coupling.[3] In detail, regional brain activation increases cerebral blood flow, bringing in highly oxygenated blood. This leads to an increase in the oxyhemoglobin concentration and a decrease in deoxyhemoglobin concentration at the site of the activation. Since deoxyhemoglobin is paramagnetic, a decrease in deoxyhemoglobin leads to an increase in the BOLD fMRI signal. The BOLD signal reflects slow neurovascular coupling, not representing the fast signals such as the neuronal activities. For the resting state data (no task is given), the signal is con fined in the low-frequency range (0.01–0.08 Hz).[4–8] In addition to BOLD contrast, there are other sources of signal in the fMRI data, which can stem from: the inflow effect, proton density effect, and partial volume effect. These effects are reflective of physiological processes. They can influence the fMRI signal directly and can also couple with the deoxyhemoglobin concentrations (eg, a change in cerebral blood flow) and affect the BOLD signal.[9–11]

The systemic low-frequency oscillation (sLFO) signals are from some physiological processes (still not clear). They are widely presented in the fMRI signals and are in the same frequency band as most of the resting state BOLD signals of neuronal origins. Highly correlated sLFOs are found in the fMRI data throughout the brain with delays.[12] The delay times between these sLFOs in different cerebral regions are primarily consistent with blood arrival time differences obtained from bolus tracking, ie, dynamic susceptibility contrast MRI.[13] In a previous study,[14] a novel method was developed to study the sLFO fMRI signals in the large arteries (ie, internal carotid artery: ICA) from resting state data. The study con firmed that 1) the sLFO signals have an extracerebral origin; 2) they travel through the arteries (ICA), capillaries (GMean), and veins (ie, superior sagittal sinus: SSS); and 3) the delays between the sLFO signals from ICA and the SSS are consistent with the cerebral circulation time (CCT: time of bolus traveling from the ICA to the SSS). However, those findings were only derived from one subject's fMRI data. The repeatability of this method needs to be established. Moreover, it is of great interest to explore its applications in assessing the age/gender differences in the cerebrovascular parameters, such as CCT. Lastly, the source of the sLFO signal in fMRI is still not clear.

Materials and Methods

In this study we applied the method (with improved registration) on a large population of healthy adults (Human Connectome Project [HCP]) to further validate it. More important, we explored the potential of using the delay time (from the ICA to the SSS), which is derived from the fMRI data without a contrast agent, as a useful biomarker for brain perfusion (although internal jugular vein [IJV] is more commonly used to determine delay time, inconsistencies in identifying the IJV with our current method led to the use of the SSS instead). To demonstrate this, the corresponding gender differences and within-subject variations in the delay times were assessed. Moreover, we applied the method on the fMRI data of children (Adolescent Brain Cognitive Development data [ABCD]) to assess the impact of age differences on the delay times.

Data Acquisition

We acquired the unprocessed resting state scans from 1206 WU-Minn HCP subjects (HCP: a study aiming to assess the heritability of human brain functional connectivity, drawn from 1206 healthy twins and nontwin siblings aged 22–35[15]; https://www.humanconnectome.org/), as well as T_1-and T_2-weighted images (T_1w and T_2w). We used “100 unrelated healthy subjects” categorized and offered by the HCP website, which includes 400 scans in total (four resting state scans per person). We also acquired the children’s imaging data from the ABCD study (ABCD: a study aiming to track the brain development on 10,000 9–10 years old from childhood through adolescence[16]; https://data-archive.nimh.nih.gov/abcd) with the following criteria: 1) age: ~9 years old; 2) scanner: Siemens 3T (Erlangen, Germany); 3) imaging: resting state fMRI, T_1w and T_2w. With these criteria, we ended up with 56 subjects (34 boys and 22 girls) at the time of the request. Eighteen subjects were excluded based on 1) unidentifiable ICAs in either structure or functional images; 2) significant artifacts in the fMRI data (eg, ghosting artifact, missing slices). Data that represent an example of a middle-age subject were acquired from the MyConnectome dataset (http://myconnectome.org/wp/), which originally aimed to characterize brain function and metabolism fluctuations of an individual (45 years old) over a long time. Note that the MyConnectome data used here are for data visualization purposes, which cannot represent a specific age group. The acquisition parameters of these data are shown in Table 1. A request of reanalysis of the publicly available data was submitted to the university’s Institutional Review Board (IRB) office, which determined that IRB approval was not necessary.

Procedures

It is difficult to identify the large blood vessels directly from the fMRI data because of the low spatial resolution and lack of proper contrast. We must rely on the T_1w and the T_2w images (due to the inflow effect) to identify the vessels (ie, ICA and SSS), generate the masks, and use these masks to extract the corresponding fMRI signals. The fMRI signals from the ICAs and the SSS were then cross-correlated to obtain the time delays for each subject. The detailed steps can be found in the following sections.

Vessel Masks Identification

Even though large blood vessels can be identified directly from the T_1w and the T_2w images, the low contrast sometimes affects accuracy. Through experimental trials, it was found that the image calculated using the equation $\frac{T1w^2}{T2w} - \frac{T1w}{T2w^2}$ greatly improved the contrast between the large blood vessels and the surrounding tissues (updated from a previous method[14]). An example of the high-resolution masks (ICA and SSS) obtained from the equation are shown in Fig. 1a, in which the SSS is shown in blue while the ICAs are shown in red. The corresponding MatLab (MathWorks, Natick, MA) programs can be found online (https://github.com/TonglabPurdue/Systematic-low-frequency-oscillation-in-fMRI/blob/master/Delay_Map_fMRI/Blood_vessels_signal_extraction.m).

fMRI Preprocessing

All of the fMRI data were preprocessed using FSL (FMRIB Software Library[17]) to correct the motion artifact and conduct registration between the high-resolution images (eg, T_1w) and the low-resolution images (ie, resting state fMRI). Afterwards, the high-resolution vessel masks (as described in the previous section) were registered to the subject's own resting state fMRI data (Fig. 1b) to produce low-resolution vessel masks. (Given the short repetition time [TR] duration, less than 1 sec, and the use of multiband echo planar imaging [EPI] acquisition, slice timing correction is not necessary here, as the HCP preprocessing pipeline suggested.[18])

Time Series Extraction and Correlation

The low-resolution vessel masks were applied to the fMRI data to extract the corresponding time series for different blood vessels. In this step, the FSL function, "fslmeants –w," was used. The option command "w" represents "weighted," which minimizes the registration error (ie, the voxel with less registration certainty has low weight). Figure 1c shows an example of the weighted-average time series for the SSS. Finally, a bandpass filter (0.01–0.08 Hz) from MatLab (zero-lag 4th-order Butterworth filter) was applied to these time series to filter for the low-frequency signals with a fixed time window from –10 to +10 sec (the range was selected based on the real cerebral circulation time, which is about 5 sec). Afterwards, cross-correlation was performed on the low-frequency fMRI time series (whole time series were used in both HCP [14:33 min] and ABCD [5:06 min] data) for the ICA and the SSS to calculate the maximum cross-correlation coefficients (MCCC) and their corresponding delay times (Fig. 1d). For each subject, the signals from both the left and the right ICAs were cross-correlated with that from the SSS.

Minimizing Spurious Correlation

The spurious correlation is always a concern in all correlation studies, especially in cross-correlation studies.[19,20] To minimize this in our study, a statistically meaningful threshold had to be established. We calculated the MCCCs among intentionally mismatched time series from different subjects of the HCP data. The values of these MCCCs (from totally unrelated time series) only reflect the spurious errors in the calculation. In particular, 1) We ranked the subjects in random orders; 2) From this order, we calculated the MCCCs from

one subject's ICA data with the following subject's SSS data (eg, subject 1's ICA data with subject 2's SSS data). The mismatched MCCCs were calculated from subject 1 to subject 100 (each subject had four resting state scans). The whole procedure (two steps) was iterated 1000 times. The MCCC threshold was then determined to minimize the spurious correlation. The threshold determined here is the only criterion for selecting qualified data that were used for further analyses, such as gender comparison, within-subject delay time variation analysis, and age comparison.

Analyses of Qualified Data

The MCCC and delay time differences caused by gender differences (F: 54, M: 46) were tested. The standard deviation (SD) of MCCC and delay times from multiple scans were calculated in each subject to represent the within-subject variation. We only selected the subjects who had three or four qualified fMRI data (passing the threshold) to get meaningful SDs. The number of selected subjects was 78 out of 100 (all from the qualified data). The distributions of these SDs and the corresponding log-logistic fitting curves were plotted. To assess the age differences, we calculated the delay times (ICA and SSS) for 38 9-year-old children (ABCD data) and compared them with the delay times of young adults from the HCP dataset (~30 years old). As a representation of the middle-age group, the results from the MyConnectome project (45-year-old single male subject with 45 resting fMRI scans) from a previous study[14] was also included. It is to be noted that about 50% of the MyConnectome data were recorded after the subject had coffee. These portions of the data were excluded since the coffee could become a confounding variable affecting vascular flow.

Model Simulation

Due to the lack of deoxyhemoglobin in large arteries, BOLD is unlikely to be the main contrast in fMRI signal from ICAs. We hypothesized that the "partial volume effect" could be the origin of the sLFOs instead of the BOLD contrast. Compared with other resting state analyses, the unique features of this fMRI study are as follows: 1) large blood vessels are the focus of the study. The diameters of ICAs and SSSs are about 5 mm, which covers 2–3 voxels (voxel size: 2 × 2 × 2 mm in HCP data). 2) When studying large vessels, the oxygen saturation (Y) is fixed. For example, the Y in the ICA is about 100%, while it is about 60% in the SSS. It is different from the common BOLD effect, where the Y changes according to neuronal activation. Therefore, we employed a model proposed by Haacke et al[11] to test the hypothesis.

Statistical Analysis

We performed *t*-tests on the MCCC and delay time to test gender differences. As for the age difference, since the qualified data do not follow normal distributions, multicomparison was achieved using the Kruskal–Wallis test at a 1% significance level.

Results

Spurious Correlation

The distribution of the total MCCCs (around 400,000) is shown in Fig. 2a, in which the MCCCs are mostly clustered around –0.2 and 0.2. Figure 2b shows the *P*-values associated

with the MCCCs. In the cases that the MCCC < –0.3 (or MCCC > 0.3), the *P*-value is less than 0.008 (ie, significant). Therefore, we selected –0.3 as our threshold of the MCCC to prevent spurious correlations (most of our results have negative MCCCs; data with MCCCs > 0.3 are explained in the Discussion). Furthermore, in the bottom panel (Fig. 2c) the distribution of the corresponding delay times of all MCCCs is shown. The delay times are evenly distributed within the cross-correlation window (ranging from – 10 to 10 sec), which was predicted based on the fact that all the time series are unrelated. The two high concentrations of delay times at the boundaries (–10 sec and 10 sec) are the result of the cross-correlation window, which "forced" the delay times outside the window to "pile" up at the boundary. This result not only offers a sufficient threshold, but also demonstrates that the spurious correlation would lead to an even distribution of delay times. Thus, highly uneven delay distributions, as shown in Fig. 3, are less likely the result of spurious correlation.

Robustness Results From HCP Data

Figure 3 demonstrates the scatterplots and histograms of the MCCCs and their corresponding delay times between the ICAs (both sides) and the SSSs among 100 subjects. Each subject has four resting state scans, resulting in 400 data points in total. The data points that do not pass the criteria are represented as blue crosses (–0.3 < MCCC < 0.3, ~15%) and black circles (MCCC > 0.3, ~5%), while the qualified data points (MCCC < –0.3) are represented as red circles. About 80% (left ICA: 79.8%; right ICA: 79.5%) of the data points passed the criteria. For the rest of the study, we only used these qualified data. The mean and the SD of the MCCCs and the delay times are: 1) –0.67 ± 0.17 (MCCC) and –5.21 ± 1.27 sec (delay time) for the left ICA and the SSS; 2) –0.63 ± 0.17 (MCCC), –5.45 ± 1.35 sec (delay time) for the right ICA and the SSS. There was no apparent difference between the results obtained for the left and the right ICAs, which is expected due to the anatomical symmetry in the blood flows of healthy subjects. The result validates that both identification and registration were correctly done. A negative delay time indicates that the sLFO fMRI signal from the ICA leads that of the SSS. Since SSS is long, there are slight differences in delay times (<1.5 sec) from different sections of the SSS (eg, the anterior part and the posterior part). However, given the inconsistency of the length of the identifiable SSS masks across subjects, we used the entire identified SSS to improve the signal-to-noise ratio (SNR). As a comparison, an example of X-ray angiography data (see Supplemental Material Fig. S2) is provided showing a flow of contrast bolus injected directly into the ICA. The series of images show the propagation of the contrast flowing through the right ICA, middle cerebral and anterior arteries, capillary bed, and the SSS. The bolus passage time from the ICA to the middle section of the SSS is roughly 4.5 sec (judging by the falling edges of the curves in the bottom graph of Supplemental Material Fig. S2). The MCCC and delay time scatterplot is shown in Fig. 3e. The qualified data (MCCC < – 0.3) were clustered around where the delay time is around 5 sec. Data within two red lines (–0.3 < MCCC < 0.3) were considered statistically insignificant, which is also reflected in their corresponding delay times spreading across the whole time window (from –10 sec to 10 sec). As for data with MCCC > 0.3, there is a small portion clustered around 2.5 sec, which is probably due to the "periodical effect"[14]; a detailed explanation is given in the Discussion.

Gender Comparison and Within-Subject Delay Time Variation

Figure 4a shows the delay time distribution (between the left ICA and the SSS) comparison between males and females (from the qualified data). The data for the females is shown on the left in red. In this figure, the delay times for both genders are normally distributed. The two-tailed *t*-test shows that there is no significant difference between the two genders in terms of their delay times ($P = 0.9846$, $P = 0.2288$ for left and right side, respectively; only the results from the left ICAs are shown). Figure 4b,c shows the distribution of within-subject MCCC and delay time variation and their corresponding fitting curves (normal for MCCC and log-logistic for delay time), which is represented by the SD of the MCCCs/delay times obtained from the three to four fMRI scans of each subject (78 out of 100 subjects' data were used). For all 78 subjects, the MCCC and the delay time variation at the 5% confidence level is 0.26 and 2.23 sec, respectively.

ABCD Data

Similar to Fig. 3, Fig. 5 shows the plots and histograms of the MCCCs and their corresponding delay times between the ICAs (both sides) and the SSSs from the ABCD dataset (38 subjects; 140 scans in total). About 53% (left ICA: 57.1%; right ICA: 49.3%) of the data points passed the criteria. About 32% of data (blue crosses) have positive MCCCs that are greater than 0.3. The mean and the SD of the MCCCs and delay times from the qualified data are: 1) –0.60 ± 0.16 (MCCC) and –4.39 ± 3.53s (delay time) for the left ICA and the SSS; 2) –0.62 ± 0.13 (MCCC), –4.58 ± 2.62 sec (delay time) for the right ICA and the SSS. The delay times are shorter compared with the results of the HCP, while no differences were found between using the left ICA and the right ICA in the calculations.

Delay Times Associated With Age

The delay time variations related to age differences were statistically analyzed using the subjects from the ABCD and the HCP dataset. Figure 6a shows boxplots of the delay times with age and gender (results from ABCD: 9–10 years old, HCP: 22–36 years old). Since we did not include other age groups in this study, the corresponding result of the MyConnectome project (single 45-year-old male subject) from a previous study was shown and serves as an example of a middle-age subject. The mean and SD of the delay times for the ABCD (38 subjects), the HCP (100 subjects), and the MyConnectome (one subject with 45 scans) are –4.48 ± 3.13 sec, –5.33 ± 1.31 sec, –7.20 ± 0.94 sec, respectively. The results show significant differences between each other (all three *P*-values are less than 0.01, with Bonferroni correction) (Fig. 6b). The linear fits, as represented by the dotted trend lines (female in red, male in blue in Fig. 6a) clearly demonstrate a positive correlation between the delay time and age, indicating that the delay time becomes larger with age (ie, the fitting is valid even without MyConnectome results).

Model Simulation

Figure 7 shows the simulation result of fMRI signal $S(\lambda, \varphi_b)$ as λ (ie, vessel dilation) goes from 0 to 1 in the cases of artery (red) and vein (blue). We found that an increase in λ would always lead to an increase in the blood fMRI signal (ie, S_b) and a decrease in the gray matter fMRI signal (ie, S_g), shown as the blue and red dots in Fig. 7b,c. However, in the case of a

highly oxygenated artery (Fig. 7c), the vessel dilation triggers a much bigger fMRI signal increase compared with that of a vein (deoxyhemoglobin in the vein is the main reason). As a result, the overall fMRI signal increases in the ICA and decreases in the SSS (as long as $\lambda < 0.8$) as these vessels dilate. In summary (Fig. 7d), we found that the vessel dilation in pixels causes opposite fMRI signal changes depending on the vessel type. The detailed information of the model can be found in the Supplemental Materials.

Discussion

In this study we demonstrated that 80% of the data (400 resting state scans) have significant negative cross-correlation coefficients (< −0.3) between the sLFOs from the ICAs and the SSSs among the 100 unrelated healthy subjects' fMRI data from the HCP with the corresponding delay times about –5 sec (the sLFO signal of the ICA leads that of the SSS). These features demonstrate the robustness of the underlying physiology among healthy subjects. The delay time (~5 sec) matches the CCT obtained by other methods. For example, Hoffmann et al[21] found that the CCT was 5.6 ± 1.7 sec, without significant side-to-side differences among healthy subjects using an ultrasound method with a galactose-based echo-contrast agent (ie, Levovist). Most recently, Liu et al[22] found the CCT interval between the ICA and the IJV for the start time and the peak filling time was 6.3 ± 1.3 sec, and 7.8 ± 2.5 sec, respectively, using ultrasound with the contrast agent Sonovue in 67 healthy subjects (33–72 years old). The X-ray angiography data offers direct convincing evidence, in which the contrast bolus was directly injected into the ICA and followed throughout the brain. Moreover, the result that no significant difference between the two genders in delay times matches the previous CCT study using contrast-enhanced Doppler sonography.[21] In this study we focused on the sLFOs in the large blood vessels. However, these signals are widely presented in the BOLD throughout the whole brain. Previous fMRI studies have validated the finding and used the sLFOs to track cerebral blood flow throughout the brain.[12,14,23] The small within-subjects delay time variation indicates that the delay time is a consistent parameter that does not change with time under the same condition due to the autoregulation of the cerebral blood flow.[24,25] Shorter delay times from the ABCD, compared with those from the HCP, implied that the delay times are shorter in children (~9 years old) than in young adults (~30 years old), which is consistent with previous studies. Wu et al[26] found that cerebral vascular peak velocities in the ICAs reached a maximum at ~6 years of age and declined thereafter (with slower rate after ~20 years of age). A similar trend was also observed in large veins, such as the SSS, but with a smaller magnitude. Decreased cerebral peak velocities in the large blood vessels could prolong the CCTs. They did not find any significant differences in any cerebral and cardiac flow/structure parameters between genders, which also matches the observations in our study.

Our simulation result shows that the same volume change in ICAs and SSSs can cause opposite fMRI signals due to the partial volume effect. One possible physiological process that produces the spontaneous oscillation in the tone of blood vessel walls (volume) is vasomotion, which is independent of the heartbeat, respiration, and neuronal activations. It has been shown that vasomotion can travel to different regions of the human brain cortex along blood vessels.[27] A similar traveling wave was also found in mice.[28] Other physiological processes related to the cardiac pulsation may have effects on the sLFO

signals. However, no direct links were found between aliased cardiac pulsation wave and heart rate variability with the sLFOs.[29]

Even though most data show significant negative cross-correlations present between sLFOs from ICAs and SSSs, there is still a small portion of the data that does not. The possible reasons are as follows. First, the "periodic-effect,"[14] in which some of the sLFOs are dominated by one low-frequency component. The MCCC calculated from this periodic signal can be either positive or negative (influenced by factors such as noise) with the corresponding delay times differing by half of the period. The ABCD data are more affected by this than the HCP data. Second, the low SNR in the arterial fMRI signal. Some contributing factors for the low SNR are: 1) Motion: ICA, as one of the largest arteries leading to the brain, is prone to the motion of the vessel wall, eg, heart pulsation. 2) The short section of the ICA in the fMRI scan: since arteries are not the focus of many studies, the fMRI scan has limited coverage of the ICAs. 3) Low-intensity fMRI signal in the arteries. These factors are even more problematic for the ABCD data. It is well known that motion artifact is a big problem in young children's data. More important, their ICAs are much narrower compared with those of adults, which makes it harder to identify them accurately. Furthermore, the fewer voxels present in the children's ICA (due to the small size) decreases the effectiveness of averaging. Lastly, shorter signal length (shorter scan time) in ABCD than that in HCP data decreases the SNR. All these factors lead to less percentage of qualified data and the larger within-subject variation in the ABCD data.

There are some limitations in this study. First, based on the pipeline of the HCP,[18] an unwarping procedure is necessary on the T_1w, T_2w, and the fMRI data to correct for the gradient distortion. However, the correlation results did not improve. One possible reason is that the interpolation of the imaging data as the result of gradient correction decreases the SNR, leading to the suboptimal outcomes. Since we do not fully understand this issue, the gradient distortion correction was not utilized in this study. Second, in the age comparison the sample size in the children (ABCD data) is less than that in the young adults (HCP). Also, a healthy middle-age population is needed to have a complete comparison of the aging effect. Lastly, an improved method is necessary to consistently identify the IJV for future analysis.

In conclusion, we have demonstrated the potential that the sLFO fMRI signals can be used as an intrinsic contrast bolus to track the cerebral blood flow. Moreover, we found that the delay times: 1) are highly consistent in each subject; 2) have no significant gender difference (among healthy young subjects); and 3) become longer with age. Lastly, from the simulations of the fMRI signal, the sLFOs likely reflect the partial volume changes in the blood vessels caused by vasomotion. This study deepens our understanding of the fMRI signal and demonstrates a method to derive perfusion parameters, such as the CCT, from fMRI data. This could potentially be used to assess some cerebrovascular diseases, such as stroke, Alzheimer's, dementia, and steno-occlusive arterial disease,[30–32] in addition to functional activations.

Supplementary Material

Refer to Web version on PubMed Central for supplementary material.

Acknowledgments

Contract grant sponsors: The ABCD Study is supported by the National Institutes of Health (NIH) and additional federal partners; Contract grant numbers: U01DA041022, U01DA041028, U01DA041048, U01DA041089, U01DA041106, U01DA041117, U01DA041120, U01DA041134, U01DA041148, U01DA041156, U01DA041174, U24DA041123, U24DA041147, U01DA041093, and U01DA041025; Contract grant sponsor: NIH; Contract grant number: K25 DA031769 (to Y.T.).

The data were provided in part by the Human Connectome Project, WU-Minn Consortium the Principal Investigators: David Van Essen and Kamil Ugurbil; (1U54MH091657) funded by the 16 NIH Institutes and Centers that support the NIH Blueprint for Neuroscience Research; and by the McDonnell Center for Systems Neuroscience at Washington University. Data used in the preparation of this article were obtained from the Adolescent Brain Cognitive Development (ABCD) Study (https://abcdstudy.org), held in the NIMH Data Archive (NDA). This is a multisite, longitudinal study designed to recruit more than 10,000 children age 9–10 and follow them over 10 years into early adulthood. A full list of supporters is available at https://abcdstudy.org/federal-partners.html. A listing of participating sites and a complete listing of the study investigators can be found at https://abcdstudy.org/Consortium_Members.pdf. ABCD consortium investigators designed and implemented the study and/or provided data but did not necessarily participate in analysis or writing of this report. This manuscript reflects the views of the authors and may not reflect the opinions or views of the NIH or ABCD consortium investigators. We also like to thank Dr. Poldrack for creating and sharing the MyConnectome dataset.

References

1. Matthews P, Jezzard P. Functional magnetic resonance imaging. J Neurol Neurosurg Psychiatry 2004;75:6–12. [PubMed: 14707297]
2. Heeger DJ, Ress D. What does fMRI tell us about neuronal activity? Nat Rev Neurosci 2002;3:142. [PubMed: 11836522]
3. Logothetis NK, Wandell BA. Interpreting the BOLD signal. Annu Rev Physiol 2004;66:735–769. [PubMed: 14977420]
4. Egorova N, Veldsman M, Cumming T, Brodtmann A. Fractional amplitude of low-frequency fluctuations (fALFF) in post-stroke depression. NeuroImage Clin 2017;16:116–124. [PubMed: 28794972]
5. Hao H, Yuxiang Y, Wenjing Z, Bo H. Sensorimotor network parcellation for pre-surgical patients using low-pass filtered fMRI. In: 2017 39th Annual International Conference of the IEEE Engineering in Medicine and Biology Society (EMBC). 2017 pp 4479–4482.
6. Feng T, Feng P, Chen Z. Altered resting-state brain activity at functional MRI during automatic memory consolidation of fear conditioning. Brain Res 2013;1523:59–67. [PubMed: 23726994]
7. Peltier SJ, Polk TA, Noll DC. Detecting low-frequency functional connectivity in fMRI using a self-organizing map (SOM) algorithm. Hum Brain Mapp 2003;20:220–226. [PubMed: 14673805]
8. Anderson JS. Origin of synchronized low-frequency blood oxygen level-dependent fluctuations in the primary visual cortex. AJNR Am J Neuroradiol 2008;29:1722–1729. [PubMed: 18635612]
9. Kim S-G, Bandettini PA. Principles of functional MRI In: Faro SH, Mohamed FB, eds. Functional MRI: Basic principles and clinical applications. New York: Springer; 2006 p 3–23.
10. Kim S-G, Ogawa S. Biophysical and physiological origins of blood oxygenation level-dependent fMRI signals. J Cereb Blood Flow Metab 2012;32:1188–1206. [PubMed: 22395207]
11. Haacke E, Lai S, Yablonskiy D, Lin W. In vivo validation of the BOLD mechanism: A review of signal changes in gradient echo functional MRI in the presence of flow. Int J Imaging Syst Technol 1995;6:153–163.
12. Tong Y, Frederick BD. Tracking cerebral blood flow in BOLD fMRI using recursively generated regressors. Hum Brain Mapp 2014;35: 5471–5485. [PubMed: 24954380]

13. Tong Y, Lindsey KP, Hocke LM, Vitaliano G, Mintzopoulos D, Frederick BD. Perfusion information extracted from resting state functional magnetic resonance imaging. J Cereb Blood Flow Metab 2017; 37:564–576. [PubMed: 26873885]
14. Tong Y, Yao JF, Chen JJ, Frederick BD. The resting-state fMRI arterial signal predicts differential blood transit time through the brain. J Cereb Blood Flow Metab 2018:271678X17753329.
15. Van Essen DC, Smith SM, Barch DM, Behrens TEJ, Yacoub E, Ugurbil K. The WU-Minn Human Connectome Project: An overview. NeuroImage 2013;80:62–79. [PubMed: 23684880]
16. Casey B, Cannonier T, Conley MI, et al. The adolescent brain cognitive development (ABCD) study: Imaging acquisition across 21 sites. Dev Cogn Neurosci 2018 [Epub ahead of print].
17. Jenkinson M, Beckmann CF, Behrens TE, Woolrich MW, Smith SM. Fsl. Neuroimage 2012;62:782–790. [PubMed: 21979382]
18. Glasser MF, Sotiropoulos Sn Fau, Wilson JA, et al. The minimal preprocessing pipelines for the Human Connectome Project. (1095–9572 (Electronic)).
19. Hocke LM, Tong Y, Lindsey KP, Frederick BD. Comparison of peripheral NIRS LFOs to other denoising methods in resting state functional fMRI with ultra-high temporal resolution. Magn Reson Med 2016;76: 1697–1707. [PubMed: 26854203]
20. Power JD, Barnes KA, Snyder AZ, Schlaggar BL, Petersen SE. Spurious but systematic correlations in functional connectivity MRI networks arise from subject motion. Neuroimage 2012;59:2142–2154. [PubMed: 22019881]
21. Hoffmann O, Weih M, Schreiber S, Einhaupl KM, Valdueza JM. Measurement of cerebral circulation time by contrast-enhanced Doppler sonography. Cerebrovasc Dis 2000;10:142–146. [PubMed: 10686453]
22. Liu X, Yang YL, Sun SG, et al. A new method of measurement of cerebral circulation time: Contrast-enhanced ultrasonography in healthy adults and patients with intracranial shunts. Ultrasound Med Biol 2014; 40:2372–2378. [PubMed: 25018026]
23. Tong Y, Lindsey KP, Hocke LM, Vitaliano G, Mintzopoulos D, Frederick BD. Perfusion information extracted from resting state functional magnetic resonance imaging. J Cereb Blood Flow Metab 2017; 37:564–576. [PubMed: 26873885]
24. Aaslid R, Lindegaard K-F, Sorteberg W, Nornes H. Cerebral autoregulation dynamics in humans. Stroke 1989;20:45–52. [PubMed: 2492126]
25. Hilz M, Stemper B, Heckmann J, Neundörfer B. Mechanisms of cerebral autoregulation, assessment and interpretation by means of transcranial Doppler sonography. Fortschr Neurol Psychiatr 2000;68:398–412. [PubMed: 11037638]
26. Wu C, Honarmand AR, Schnell S, et al. Age-related changes of normal cerebral and cardiac blood flow in children and adults aged 7 months to 61 years. J Am Heart Assoc 2016;5.
27. Rayshubskiy A, Wojtasiewicz TJ, Mikell CB, et al. Direct, intraoperative observation of ~0.1 Hz hemodynamic oscillations in awake human cortex: Implications for fMRI. Neuroimage 2014;87:323–331. [PubMed: 24185013]
28. Bumstead JR, Bauer AQ, Wright PW, Culver JP. Cerebral functional connectivity and Mayer waves in mice: Phenomena and separability. J Cereb Blood Flow Metab 2017;37:471–484. [PubMed: 26868180]
29. Hocke LM, Tong Y, Lindsey KP, De B, Frederick B. Comparison of peripheral near-infrared spectroscopy low-frequency oscillations to other denoising methods in resting state functional MRI with ultrahigh temporal resolution. Magn Reson Med 2016;76:1697–1707. [PubMed: 26854203]
30. Schreiber SJ, Franke U, Doepp F, Staccioli E, Uludag K, Valdueza JM. Doppler sonographic measurement of global cerebral circulation time using echo contrast-enhanced ultrasound in normal individuals and patients with arteriovenous malformations. Ultrasound Med Biol
31. Schreiber SJ, Doepp F, Spruth E, Kopp UA, Valdueza JM. Ultrasonographic measurement of cerebral blood flow, cerebral circulation time and cerebral blood volume intravascular and Alzheimer's dementia. J Neurol 2005;252:1171–1177. [PubMed: 16151603]
32. Lin CJ, Hung SC, Guo WY, et al. Monitoring peri-therapeutic cerebral circulation time: A feasibility study using color-coded quantitative DSA in patients with steno-occlusive arterial disease. Am J Neuroradiol 2012;33:1685. [PubMed: 22499839]

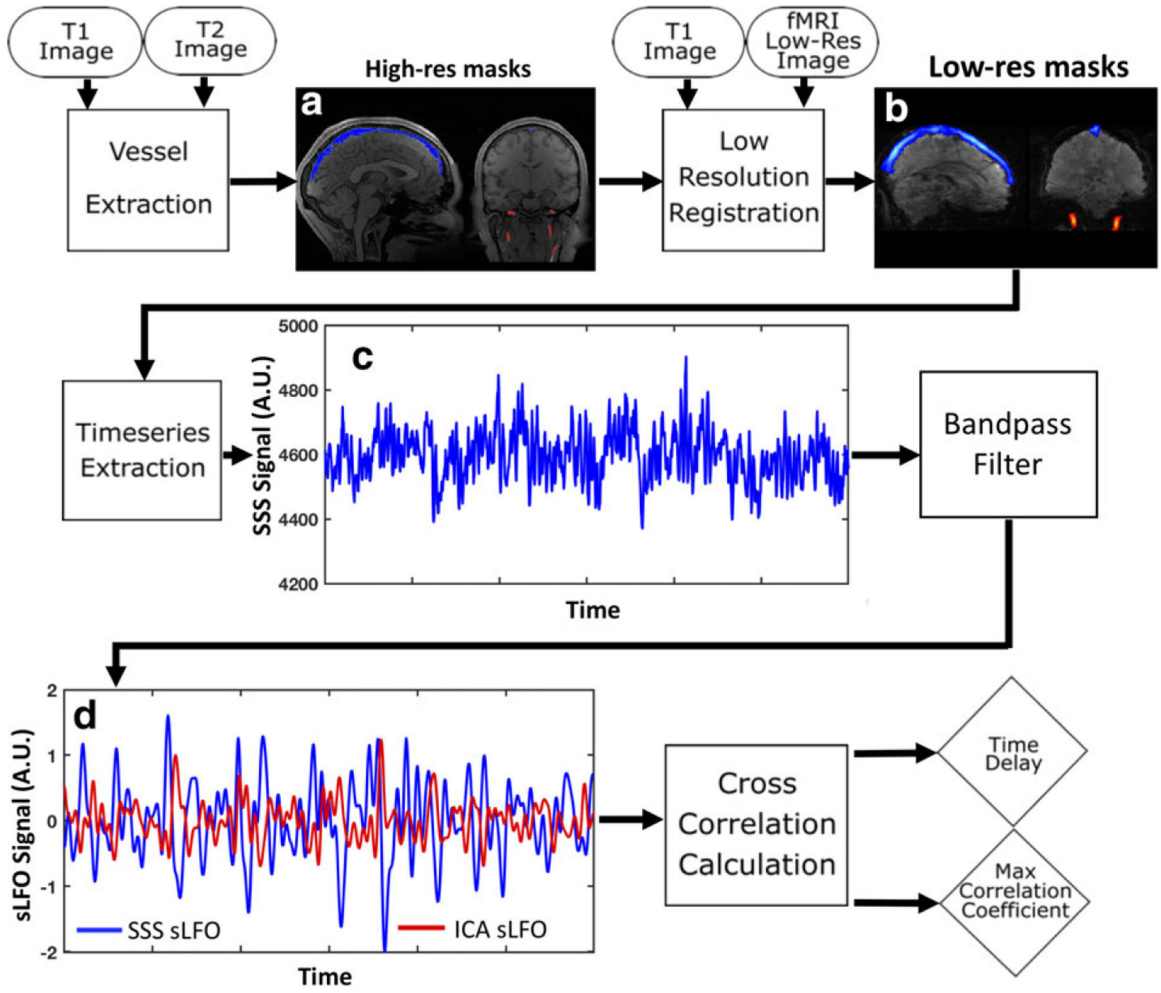

FIGURE 1:

The flow chart of the data processing and analytical procedure. **(a)** High-resolution masks of the superior sagittal sinus (SSS) and the internal carotid arteries (ICAs) generated from T_1- and T_2-weighted images. **(b)** Low-resolution masks of the SSS and the ICAs (registered from high-resolution masks). **(c)** An example time series extracted from the fMRI signal of the SSS. **(d)** The example sLFOs from fMRI signals of the ICA and the SSS after filtering (0.01–0.08 Hz).

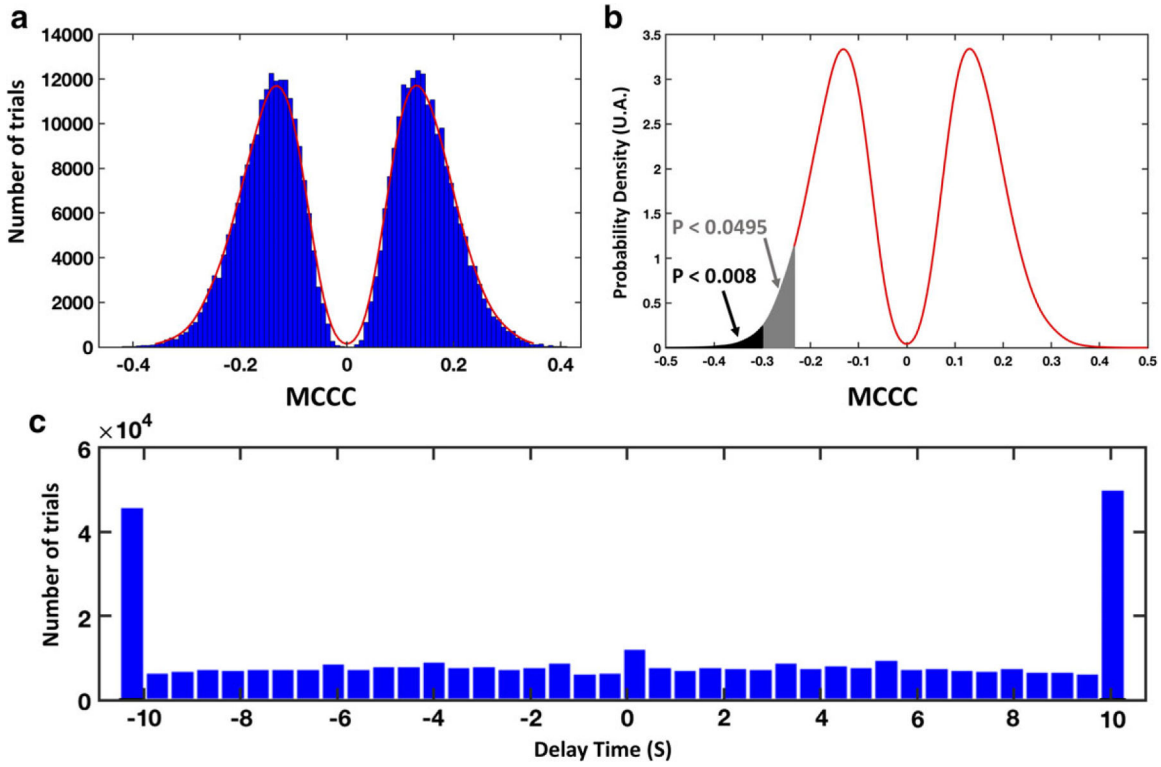

FIGURE 2:

Results in the maximum cross-correlation coefficients (MCCCs) and their corresponding delay times using mismatched time series from different subjects randomly selected.

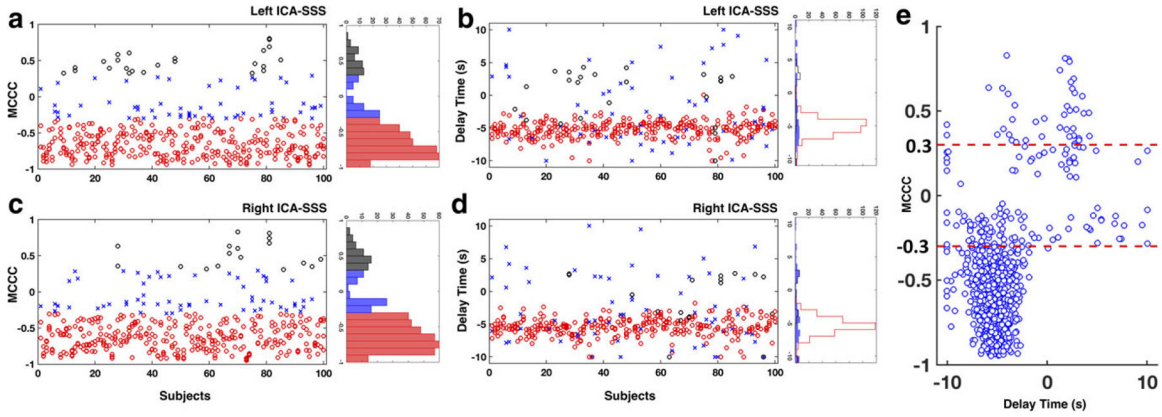

FIGURE 3:

The scatterplots of the MCCCs (in **(a,c)**) and their corresponding delay times (in **(b,d)**) of 100 subjects (each subject had four scans, resulting in four points for each subject in the graph). The results using the data from the left ICAs and SSSs are shown at the top (a,b), while the results using the data from the right ICAs and SSSs are shown at the bottom **(c,d)**. Red circles are the results with MCCC < –0.3 (left: 79.8%, right: 79.5%). Black circles are the results with MCCC > 0.3 (left: 6%, right: 4.8%). Blue crosses are the results with –0.3 < MCCC < 0.3 (left:14.2%, right:15.7%). The corresponding distribution is displayed next to each plot. The scatterplot for the MCCCs and the delay times are shown in **(e)**.

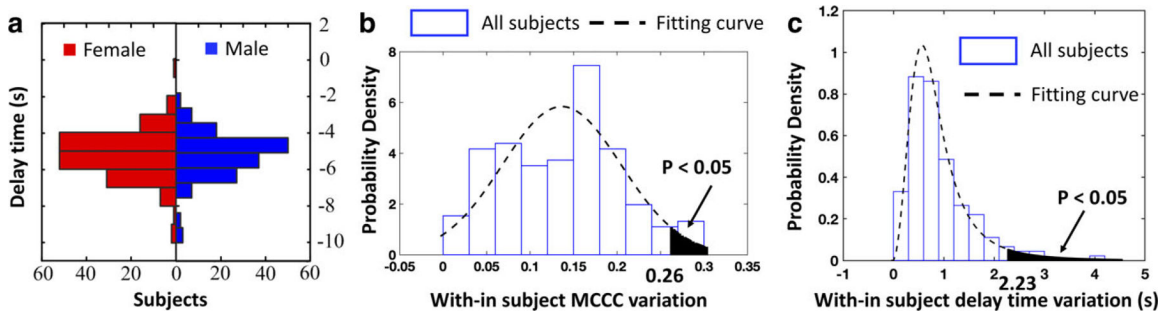

FIGURE 4:

The distribution of delay times between male (blue) and female (red) are shown in **(a)** (results using data from left ICAs and SSSs). The probability density of within subject MCCC and delay time variations and their respective fitting curves (dashed line) are shown in **(b,c)**.

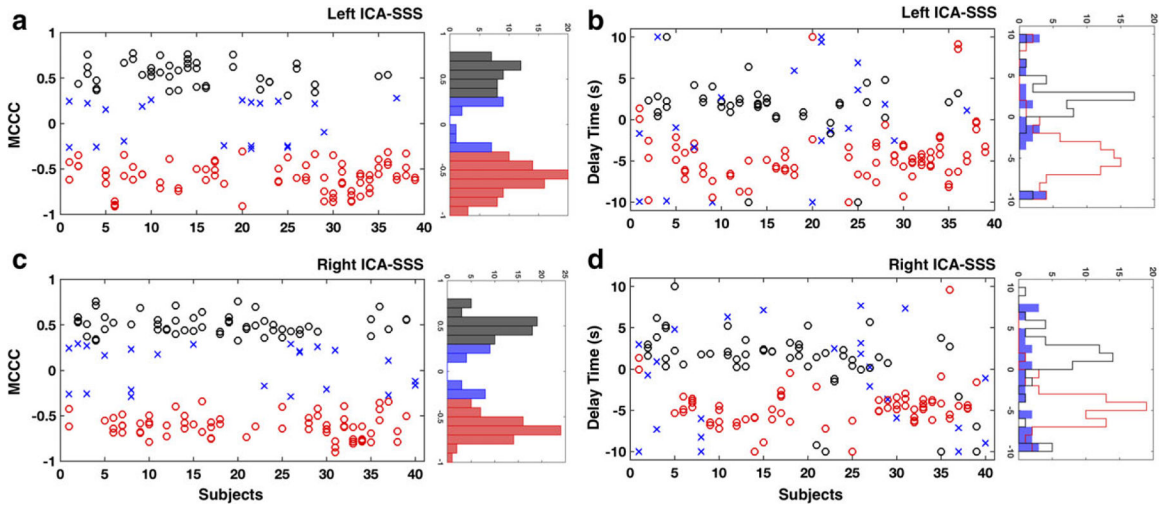

FIGURE 5:

The scatterplots of the MCCCs (in **(a,c)**) and their corresponding delay times (in **(b,d)**) of ABCD data (38 subjects). The results using the data from left ICAs and SSSs are shown at the top **(a,b)**, while the results using the data from right ICAs and SSSs are shown at the bottom **(c,d)**. Red circles are the results with MCCC < –0.3 (left: 57.1%, right: 49.3%). Black circles are the results with MCCC > 0.3 (left: 29.3%, right: 34.3%). Blue crosses are the results with –0.3 < MCCC < 0.3 (left:13.6%, right:16.4%). The corresponding distribution is displayed next to each plot.

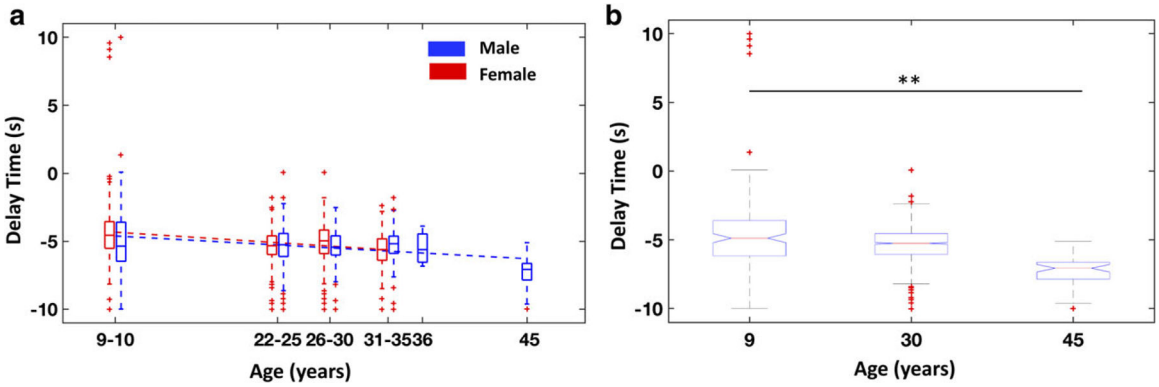

FIGURE 6:

The age effects on delay times from different groups. Boxplots of delay times with age and gender (results from ABCD (Adolescent Brain Cognitive Development)): 9–10 years old, HCP (Human Connectome Project): 22–36 years old and MyConnectome: 45 years old; MyConnectome result serves as an example of a middle-age subject) are shown in **(a)**. Statistical multicomparison using a Kruskal–Wallis test at the 1% significance level and the corresponding box plot are shown in **(b)**.

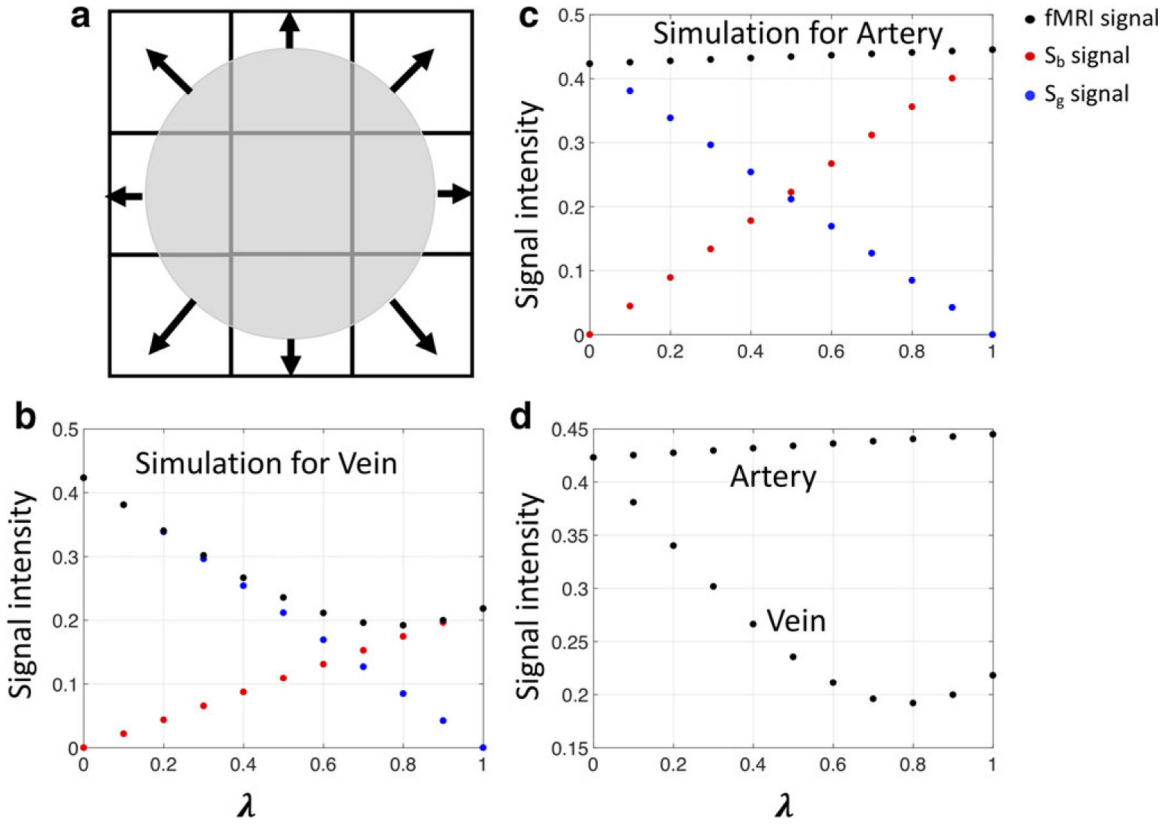

FIGURE 7:

The simulation results of the partial volume effects on fMRI signal. Illustration of the partial volume effect of the large blood vessel is shown in **(a)**. The variations of simulated intravascular (Sb), gray matter (Sg), and combined the fMRI signals caused by partial volume change are shown in **(b)** for the vein and **(c)** for the artery. The changes of the combined fMRI signals (in arteries and veins) is shown again in **(d)**.

TABLE 1.

List of Scan Parameters of fMRI and Anatomical Images of the Human Connectome Project (HCP), the Adolescent Brain Cognitive Development (ABCD) Data, and the Myconnectome Data

Item dataset	T1-weighted HCP / ABCD / Myconnectome	T2-weighted HCP / ABCD / Myconnectome	fMRI HCP / ABCD / Myconnectome
Voxel size (mm)	0.7^3 / 1^3 / 0.7^3	0.7^3 / 1^3 / 0.7^3	2^3 / 2.4^3 / 2.4*2.4*2
TR (msec)	2400.0 / 2500 / 2400	3200 / 3200 / 3200	720 / 800 / 1160
TE (msec)	2.14 / 2.88 / 2.14	560.0 / 565 / 565	33.10 / 30 / 30
Slices per slab	256 / 176 / 256	256 / 176 / 256	72 / 60 / 68
FOV (mm)	224 / 256 / 224	224 / 256 / 224	208*180*144 / 216 / 230
Flip angle (deg)	8 / 8 /8	− / Variable	52 / 52 63
Multiband	− / − / −	− / − / −	8 / 6 / 4
Scan length (min:second)	− / 7:12 / 7:40	− / 6:35 / 8:24	14:33 / 5:06 / 10:00

J Magn Reson Imaging. Author manuscript; available in PMC 2020 April 21.